PCCP

RSC Publishing

COMMUNICATION

View Article Online
View Journal | View Issue

CH_2OO Criegee biradical yields following photolysis of CH_2I_2 in O_2†

Cite this: *Phys. Chem. Chem. Phys.*, 2013, **15**, 19119

Received 13th June 2013,
Accepted 6th September 2013

DOI: 10.1039/c3cp52466c

www.rsc.org/pccp

Daniel Stone,[a] Mark Blitz,*[ab] Laura Daubney,[a] Trevor Ingham[ab] and Paul Seakins[ab]

Yields of CH_2OO and CH_2IO_2 from the reaction of CH_2I radicals with O_2 are reported as a function of total pressure, $[N_2]$ and $[O_2]$ at T = 295 K using three complementary methods. Results from the three methods are similar, with no observed additional dependence on $[O_2]$. The $CH_2I + O_2$ reaction has a yield of ∼18% CH_2OO at atmospheric pressure.

Criegee biradicals (CR_2OO) are key reaction intermediates in the ozonolysis of unsaturated organic compounds,[1] and their involvement in the atmospheric oxidation of alkenes has long been postulated.[2,3] Despite much effort, direct observations of Criegee biradicals have only recently been reported for CH_2OO[4–8] and CH_3CHOO.[9] Photolysis of CH_2I_2 in the presence of O_2 has been shown to produce CH_2OO at low pressures through the reactions:[5,10]

$$CH_2I_2 + h\nu \rightarrow CH_2I + I \qquad (R1)$$

$$\begin{aligned} CH_2I + O_2 &\rightarrow CH_2OO + I \\ &\rightarrow CH_2IO_2 \end{aligned} \qquad (R2)$$

However, the reaction between CH_2I and O_2 proceeds *via* initial formation of an excited complex, $CH_2IOO^{\#}$, which has the potential for collisional stabilisation to produce CH_2IO_2 peroxy radicals (R2b) in competition with production of the CH_2OO Criegee biradical (R2a) (Scheme 1):[10]

$$CH_2I + O_2 \rightarrow CH_2IOO^{\#}$$

$$CH_2IOO^{\#} \rightarrow CH_2OO + I \qquad (R2a)$$

$$CH_2IOO^{\#} + M \rightarrow CH_2IO_2 + M \qquad (R2b)$$

A number of investigations by Enami and co-workers[11–13] suggested production of HCHO and IO from $CH_2I + O_2$, but other studies,[14,15,33] including measurements in this laboratory,[15] have demonstrated that the production of IO results from secondary processes, and that IO is not a direct reaction product of (R2).[14,15,33]

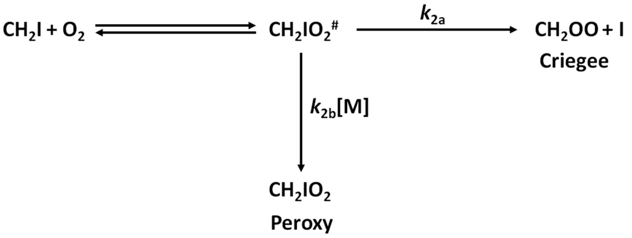

Scheme 1 Chemical activation scheme to describe the reaction between CH_2I and O_2 (R2), where the initially formed excited species $CH_2IO_2^{\#}$ either proceeds to produce $CH_2OO + I$ (k_{2a}) or is collisionally stabilised to produce the CH_2IO_2 peroxy radical or (k_{2b}[M]).

The yields of CH_2OO and CH_2IO_2 from $CH_2I + O_2$ were recently measured by Huang *et al.*[10] as a function of $[N_2]$, $[O_2]$ and [He] by monitoring the I atoms produced in (R1) and (R2a) *via* their infrared absorption owing to $F'' = 4 \rightarrow F' = 3$ of the $^2P_{3/2} \rightarrow {}^2P_{1/2}$ spin–orbit transition at 7603.138 cm^{-1}. Given the stoichiometry between CH_2I and I in (R1), it is possible to infer the fraction of CH_2I radicals producing CH_2OO through comparison of the I atom yields from the instant photolytic production in (R1) and the slower production *via* (R2a). While there is potential for multi-photon dissociation of CH_2I_2 to produce $CH_2 + 2I$, it is expected that this is relatively minor compared to production of $CH_2I + I$.[16–19] Huang *et al.* showed that the yield of CH_2OO decreases with total pressure, consistent with collisional stabilisation of the $CH_2IOO^{\#}$ intermediate to CH_2IO_2.

However, Huang *et al.* also reported significant differences in the I atom yields from (R2a) (and thus in CH_2OO yields) between experiments performed in N_2 buffer gas and those performed in O_2, indicating a much greater efficiency of O_2 for stabilisation of $CH_2IOO^{\#}$ to CH_2IO_2 compared to N_2, and an unusual interaction between $CH_2IOO^{\#}$ and O_2.

In this work we report observations of the yields of CH_2OO and CH_2IO_2 from $CH_2I + O_2$ following laser flash photolysis of CH_2I_2–N_2–O_2 gas mixtures as a function of $[N_2]$, $[O_2]$ and total

---

[a] *School of Chemistry, University of Leeds, UK. E-mail: m.blitz@leeds.ac.uk*
[b] *National Centre for Atmospheric Science, University of Leeds, UK*

† Electronic supplementary information (ESI) available. See DOI: 10.1039/c3cp52466c

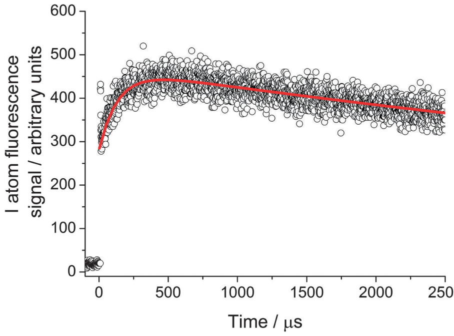

Fig. 1 Iodine atom signal following photolysis of CH_2I_2 in the presence of O_2. For this plot total pressure (N/V) = 3.27×10^{17} cm^{-3} (~10 Torr, predominantly N_2); $[O_2] = 4.02 \times 10^{15}$ cm^{-3}; $[CH_2I_2] = 5.03 \times 10^{12}$ cm^{-3}. The time resolution is such that iodine production from photolysis and reaction can be identified. The fit to eqn (1) is shown by the solid line.

pressure using several complementary methods at total pressures between 25 and 450 Torr. Experiments were initially performed to monitor I atom fluorescence, thus enabling inference of the yields of CH_2OO and CH_2IO_2 in the manner described by Huang *et al.*[10] Subsequent experiments monitored the yields of HCHO from reactions of CH_2OO–CH_2IO_2 in the presence of excess SO_2 or NO by laser-induced fluorescence (LIF) of HCHO at $\lambda \sim 353.1$ nm. Full experimental details are given in the ESI.† All experiments were performed at $T = 295$ K unless stated otherwise.

Fig. 1 shows the typical I atom signal following photolysis of CH_2I_2–O_2–N_2. The instantaneous photolytic production of iodine atoms through (R1) can be clearly distinguished from the subsequent growth in (R2a). The I atom signals were analysed using eqn (1):

$$[\mathrm{I}]_t = S_0[\exp(-k_{\mathrm{loss}}t)] + \frac{S_1 k_2'}{k_2' - k_{\mathrm{loss}}}\left[\exp(-k_{\mathrm{loss}}t) - \exp\left(-k_2' t\right)\right] \quad (1)$$

where $[\mathrm{I}]_t$ is the iodine atom signal at time t, S_0 is the amplitude of the instant photolytic signal resulting from (R1), S_1 is the amplitude of the iodine atom signal resulting from the slower growth process occurring after photolysis, k_2' is the pseudo-first-order rate coefficient for (R2) (*i.e.* $k_2' = k_2[O_2]$), and k_{loss} is the rate coefficient representing the slow loss of iodine atoms from the detection region *via* reaction or diffusion. A value of $k_2 = (1.67 \pm 0.04) \times 10^{-12}$ cm^3 s^{-1} was determined in this work (see ESI†), in agreement with previous measurements of $(1.40 \pm 0.35) \times 10^{-12}$ cm^3 s^{-1},[20] and $(1.6 \pm 0.2) \times 10^{-12}$ cm^3 s^{-1}.[21] All errors quoted for this work are statistical at the 1σ level unless stated otherwise.

The absolute iodine atom yield from reaction (R2a) is given by the ratio S_1/S_0, and was observed to decrease with increasing total pressure of N_2, consistent with production of the CH_2OO Criegee biradical at low pressures and stabilisation of the chemically activated $CH_2IO_2^{\#}$ species to the CH_2IO_2 peroxy radical at higher pressures. Solution of the I atom yield from (R2) (Φ_{I}), and thus the CH_2OO yield, is given by the Stern–Volmer relationship in eqn (2):

$$\frac{1}{\Phi_{\mathrm{I(R2)}}} = 1 + \frac{k_{2\mathrm{b}}}{k_{2\mathrm{a}}}[\mathrm{M}] \quad (2)$$

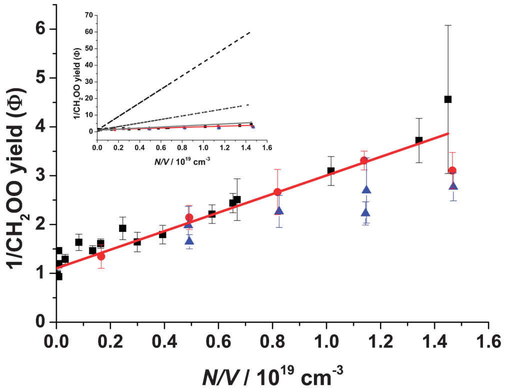

Fig. 2 Stern–Volmer analyses for CH_2OO yields from $CH_2I + O_2$ as a function of total pressure. Main panel shows results from this work monitoring iodine atom production (squares; intercept = 1.08 ± 0.12; slope = $(2.28 \pm 0.11) \times 10^{-19}$ cm^3), and HCHO production in the presence of SO_2 (triangles; intercept = 1.46 ± 0.25; slope = $(0.95 \pm 0.24) \times 10^{-19}$ cm^3) and NO (circles; intercept = 1.41 ± 0.30; slope = $(1.33 \pm 0.31) \times 10^{-19}$ cm^3). Constraining the intercepts to unity for fits to SO_2 and NO data gives slopes of $(1.37 \pm 0.10) \times 10^{-19}$ cm^3 and $(1.71 \pm 0.16) \times 10^{-19}$ cm^3, respectively. Data shown for SO_2 and NO were taken over a range of $[O_2]$ ($(0.1$–$7.8) \times 10^{18}$ cm^{-3}). A fit to all data reported in this work gives an intercept of 1.10 ± 0.23 and a slope of $(1.90 \pm 0.22) \times 10^{-19}$ cm^3 (shown by the solid line). Error bars shown on the plot and those given for the fits are 1σ, with fits weighted to the experimental errors. Separate lines of best fit for results from the different methods are not shown for clarity but are given in the ESI.† The inset plot shows results from this work together with parameterisations given by Huang *et al.* for N_2 (solid light grey line), O_2 (broken black line) and air (broken dark grey line).

where $\Phi_{\mathrm{I(R2)}}$ is the iodine atom yield from (R2) (*i.e.* S_1/S_0), $k_{2\mathrm{b}}/k_{2\mathrm{a}}$ is the Stern–Volmer quenching coefficient, and [M] is the total number density of the system.

Fig. 2 shows the Stern–Volmer plot for reaction (R2). The intercept of the iodine atom Stern–Volmer plot is 1.08 ± 0.12, consistent with channel 2a being the dominant bimolecular process. The slope of the Stern–Volmer plot gives the Stern–Volmer quenching coefficient ($k_{2\mathrm{b}}/k_{2\mathrm{a}}$), and is equal to $(2.28 \pm 0.11) \times 10^{-19}$ cm^3 for these experiments, similar to the value of $k_{2\mathrm{b}}/k_{2\mathrm{a}} = (3.1 \pm 0.2) \times 10^{-19}$ cm^3 reported by Huang *et al.*[10] for experiments in N_2 buffer gas. For stabilisation of $CH_2IO_2^{\#}$ by O_2, Huang *et al.* report a value of $k_{2\mathrm{b}}/k_{2\mathrm{a}} = (4.09 \pm 0.32) \times 10^{-18}$ cm^3. The iodine atom experiments in this work were conducted at low $[O_2]$ ($\sim 4 \times 10^{15}$ cm^{-3}) to ensure (R2a) was sufficiently slow to provide confidence in the resolution of the photolytic I atom production from the chemical I atom production. The effects of $CH_2IO_2^{\#}$ stabilisation by O_2 were thus investigated in the HCHO yield experiments.

Fig. 3a shows a typical kinetic trace for HCHO following photolysis of CH_2I_2–O_2–N_2 in the absence of any additional co-reagent (*i.e.* SO_2 or NO), in which HCHO is produced in the system by reactions (R3–R6):

$$CH_2OO + I \rightarrow HCHO + IO \quad (R3)$$

$$CH_2IO_2 + I \rightarrow CH_2IO + IO \quad (R4)$$

$$CH_2IO_2 + CH_2IO_2 \rightarrow 2CH_2IO + O_2 \quad (R5)$$

$$CH_2IO \rightarrow HCHO + I \quad (R6)$$

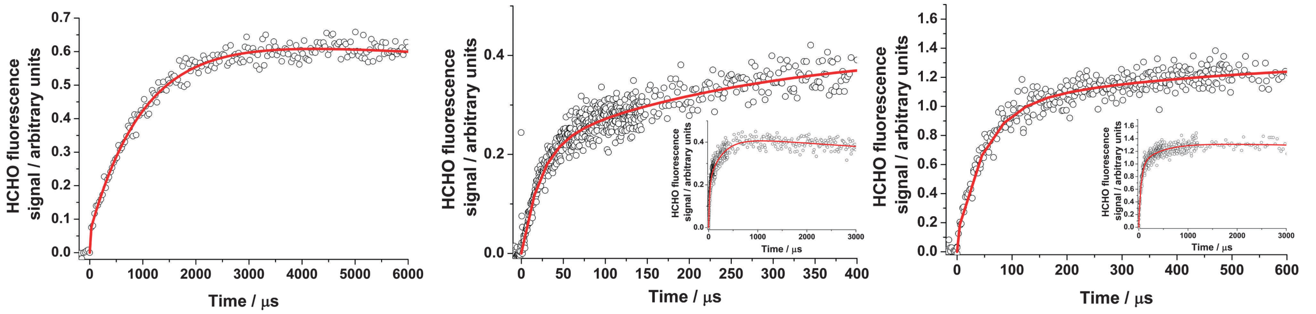

Fig. 3 HCHO fluorescence signals following photolysis of CH_2I_2 in the presence of O_2. Panel (a) shows HCHO signals at 150 Torr in the absence of any co-reagent with the fit to eqn (3). Panel (b) shows HCHO signals at 250 Torr in the presence of SO_2, with the fit to eqn (4). Panel (c) shows HCHO signals at 250 Torr in the presence of NO, with the fit to eqn (4). The inset plots in (b) and (c) show the evolution of the signals to longer times.

Although the HCHO production in this system is not strictly pseudo-first-order, Gravestock *et al.*[15] have shown that the growth from reactions (R3–R6) can be approximated to pseudo-first-order behaviour, and thus the data can be fitted using eqn (3):[14,15]

$$[\mathrm{HCHO}]_t = S_0[\exp(-k_{\mathrm{loss}}t)] + \frac{S_1 k_g{}'}{k_g{}' - k_{\mathrm{loss}}}\left[\exp(-k_{\mathrm{loss}}t) - \exp\left(-k_g{}'t\right)\right] \quad (3)$$

where $[\mathrm{HCHO}]_t$ is the HCHO signal at time t, S_0 is the amplitude of the HCHO signal at time zero, S_1 is the maximum HCHO signal, $k_g{}'$ is the pseudo-first-order rate coefficient for HCHO growth, and k_{loss} is the rate coefficient representing the slow loss of HCHO from the detection region *via* diffusion. Some initial HCHO production was observed owing to multi-photon photolysis of CH_2I_2 and the subsequent rapid reaction of $^3CH_2$ with O_2,[16–19] with S_0 typically no greater than 5–10% of S_1. In the present experiments $k_g{}'$ was typically $\sim$500 s^{-1}, which is one to two orders of magnitude slower than the reactions occurring when SO_2 or NO were added to the system. Simulations performed with the numerical integration package Kintecus[22] (provided in the ESI†) indicate that eqn (3) faithfully describes the yields of HCHO (*i.e.* S_1) in this system. Reactions (R3–R6) imply that all the CH_2OO and CH_2IO_2 react to form formaldehyde, *i.e.* all the CH_2I radicals are converted to HCHO. The recent study by Huang *et al.*[10] has demonstrated that the Criegee radical, CH_2OO, is formed with or near unity yields at low pressures from reaction (R2). The validity of 100% production of HCHO in the system can be tested at low pressures with Criegee reactions that produce formaldehyde. At low pressures the reaction between CH_2OO with SO_2 is known to produce 100% HCHO,[23] and below we demonstrate that the total HCHO yield in the system is the same with and without the addition of SO_2, only the timescale for its formation varies.

Experiments conducted in excess SO_2 or NO did not result in a decrease in the HCHO yield on addition of the co-reagent, indicating complete titration of both CH_2OO and CH_2IO_2 to HCHO. In both cases biexponential growth of HCHO was observed, as shown in Fig. 3b and c, with the observed HCHO signal in both cases described by eqn (4):

$$\begin{aligned}[\mathrm{HCHO}]_t = {} & S_0[\exp(-k_{\mathrm{loss}}t)] \\ & + \frac{S_1 f k_{g1}{}'}{k_{g1}{}' - k_{\mathrm{loss}}}\left[\exp(-k_{\mathrm{loss}}t) - \exp\left(-k_{g1}{}'t\right)\right] \\ & + \frac{S_1(1-f)k_{g2}{}'}{k_{g2}{}' - k_{\mathrm{loss}}}\left[\exp(-k_{\mathrm{loss}}t) - \exp\left(-k_{g2}{}'t\right)\right]\end{aligned} \quad (4)$$

where $[\mathrm{HCHO}]_t$ is the HCHO signal at time t, S_0 is the amplitude of the HCHO signal at time zero, S_1 is the maximum HCHO signal, $k_{g1}{}'$ is the pseudo-first-order rate coefficient for the fast HCHO growth, $k_{g2}{}'$ is the pseudo-first-order rate coefficient for the slower HCHO growth, f is the fractional contribution of the fast growth process to the total HCHO yield (and hence $(1-f)$ is the fractional contribution of the slower growth process to the total HCHO yield), and k_{loss} is the rate coefficient representing the slow loss of HCHO from the detection region *via* diffusion. f is therefore related to the yield of the Criegee, eqn (2), as we demonstrate below. Again, in experiments conducted with a photolysis wavelength of 248 nm, some initial HCHO production was observed owing to multi-photon photolysis of CH_2I_2 and the subsequent rapid reaction of $^3CH_2$ with O_2,[16–19] with S_0 typically no greater than 5–10% of S_1. In experiments using a photolysis wavelength of 355 nm, $S_0 = 0$.

For both SO_2 and NO experiments, the rate of the initial fast HCHO growth displayed a linear dependence on $[SO_2]$ or [NO], respectively, with $k_{g1}{}'$ determined over the range 5000–60 000 s^{-1}. The rate of the slower secondary growth was independent of $[SO_2]$ or [NO], and occurred at a similar rate to the HCHO growth observed in the absence of any additional co-reagent, and thus attributed to HCHO production *via* reaction (R3) or (R4–R6). The fact that $k_{g1}{}' \gg k_{g2}{}'$ means that f is reliably determined, and that $k_{g1}{}'$ is determined without any significant influence from the more complicated kinetics associated with the slower kinetics, $k_{g2}{}'$.

The fast HCHO in the presence of SO_2 is consistent with production from $CH_2OO + SO_2$:

$$CH_2OO + SO_2 \rightarrow HCHO + SO_3 \quad (R7)$$

The slower growth of HCHO occurs as a result of reactions (R4–R6). Reaction of the peroxy radical with SO_2 is unlikely,[24] and the slower HCHO growth is not dependent on $[SO_2]$. As $[SO_2]$ is in large excess over radicals in the system, k_{g1}' in eqn (4) is given by $k_{g1}' = k_7[SO_2]$, while k_{g2}' approximates the growth of HCHO through reactions (R4–R6). The returned value of f in this case is equal to the CH_2OO yield.

Reactions of peroxy radicals with NO are typically fast (for example, $k_{CH_3O_2+NO} = 7.7 \times 10^{-12}\ cm^3\ s^{-1}$ at 298 K[25]), while Welz *et al.*[5] reported an upper limit for the rate coefficient for reaction of CH_2OO with NO of $<6 \times 10^{-14}\ cm^3\ s^{-1}$. Therefore, we propose that the fast HCHO growth in experiments with NO results from the reaction of CH_2IO_2 with NO (R8) followed by the rapid decomposition of CH_2IO to HCHO and I in (R6),[15] with the slower growth resulting from (R3):

$$CH_2IO_2 + NO \rightarrow CH_2IO + NO_2 \qquad (R8)$$

$$CH_2IO \rightarrow HCHO + I \qquad (R6)$$

As [NO] is in large excess over the other radicals in the system, k_{g1}' in eqn (4) is therefore given by $k_{g1}' = k_8[NO]$, while k_{g2}' approximates the growth of HCHO through reaction (R3). The returned values f in this case are thus equal to the yields of CH_2IO_2.

While the slower growth of HCHO is not strictly pseudo-first-order, but is treated as such by eqn (4), simulations (described in the ESI†) show that the yields of HCHO from the two growth processes are well described by eqn (4) and the yields from the two processes (*i.e.* S_1 and f) are faithfully determined by fitting to eqn (4). In both systems, the rate of the fast growth process (6000–60 000 for SO_2; 5000–20 000 s^{-1} for NO) is significantly faster than that of the slower growth process ($\sim$300–500 s^{-1}), ensuring that the two growth processes are essentially decoupled and the HCHO yields from the two growth processes can be distinguished, and that the rate coefficient describing the fast growth is equal to that for the pseudo-first-order reactions, (R7) or (R8). We assign no kinetic information to k_{g2}' for either system, and as shown in the ESI,† the approximation of the slower growth process to pseudo-first-order kinetics leads to uncertainties in the yields of only 2–3%.

As noted above, there was no change in the total HCHO yield in the system upon the addition of either SO_2 or NO, and this was observed to be the case at all total pressures. At low pressures where the CH_2OO yield is close to unity, the addition of SO_2 leads to reaction (R7) and formation of HCHO with close to 100% yield.[23] In the ESI,† Fig. S3 compares the HCHO signal in the system with and without the addition of SO_2. The fact that both traces observe the same amount of HCHO in the system adds validity to the assumption that in the absence of reagents, reactions (R3–R6), lead to 100% HCHO formation. At higher total pressures where CH_2IO_2 formation is significant, the reason the HCHO yield is still 100% is because there is no reaction between the peroxy radical and SO_2, which is in agreement with the literature,[24] and the peroxy radical is titrated to HCHO *via* (R4–R6). In the case of NO, it is the peroxy radical that reacts rapidly with the NO (R8) to form HCHO, but there is no significant reaction between the CH_2OO and NO, in accord with the results from Welz *et al.*,[5] and therefore HCHO is formed on a slow timescale *via* reaction (R3). This again leads to 100% yield of HCHO in the system independent of total pressure, in accord with the data.

Thus, the fractional contributions of the fast and slow growth processes to the total HCHO yields in the presence of NO and SO_2 can be used to identify the yields of CH_2OO and CH_2IO_2 from the reaction of CH_2I with O_2. The fractional contribution of the fast growth process to the total HCHO yield in the presence of NO thus reflects the yield of CH_2IO_2 from (R2) (*i.e.* $Y_{CH_2IO_2} = k_{2b}[M]/(k_{2a} + k_{2b}[M]) = f_{NO}$ and $Y_{CH_2OO} = k_{2a}/(k_{2a} + k_{2b}[M]) = 1 - f_{NO}$), while the fractional contribution of the fast growth process to the total HCHO yield in the presence of SO_2 reflects the yield of CH_2OO from (R2) (*i.e.* $Y_{CH_2OO} = k_{2a}/(k_{2a} + k_{2b}[M]) = f_{SO_2}$ and $Y_{CH_2IO_2} = k_{2b}[M]/(k_{2a} + k_{2b}[M]) = 1 - f_{SO_2}$).

Fig. 2 also shows the Stern–Volmer analysis for CH_2OO yields determined by the SO_2 and NO experiments (*i.e.* Stern–Volmer plots for $1/f_{SO_2}$ and $1/(1-f_{NO})$, respectively). Experiments with SO_2 (triangles) give $k_{2b}/k_{2a} = (0.95 \pm 0.24) \times 10^{-19}\ cm^3$, while those with NO (circles) give $k_{2b}/k_{2a} = (1.33 \pm 0.31) \times 10^{-19}\ cm^3$, with intercepts of 1.46 ± 0.25 and 1.41 ± 0.30, respectively. Constraining the intercepts to unity in the fits to data from the SO_2 and NO experiments gives $k_{2b}/k_{2a} = (1.37 \pm 0.10) \times 10^{-19}\ cm^3$ and $k_{2b}/k_{2a} = (1.71 \pm 0.16) \times 10^{-19}\ cm^3$, respectively.

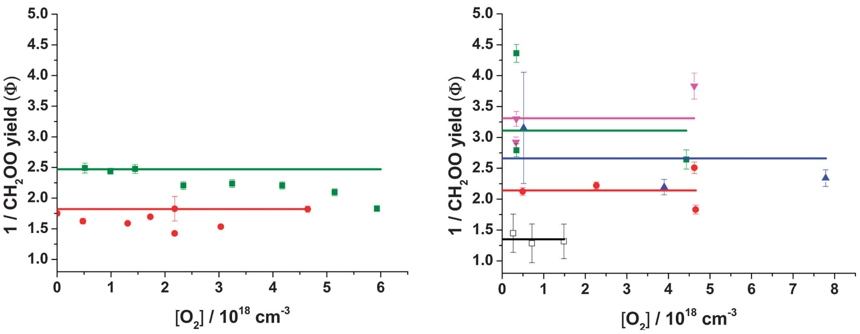

Fig. 4 Inverse of CH_2OO yields from $CH_2I + O_2$ as a function of $[O_2]$ for experiments with (a) SO_2 at 150 Torr (circles) and 350 Torr (squares); (b) NO at 50 Torr (open squares), 150 Torr (circles), 250 Torr (triangles), 350 Torr (filled squares) and 450 Torr (inverted triangles). Horizontal lines show the average inverse CH_2OO yield at each pressure for all experiments SO_2 (panel a) and NO (panel b). Error bars are 1σ in the fits to eqn (4).

Further details can be found in the ESI.† The relative errors in the SO_2 and NO experiments are typically larger than those for the iodine atom experiments owing to the need to fit a greater number of parameters in eqn (4) compared to eqn (1), and the smaller range of pressures in the Stern–Volmer plot for which the yields can be determined by the SO_2 or NO method (at low and high pressures, where one of CH_2OO or CH_2IO_2 dominates the HCHO growth it is difficult to resolve the two growth components, and thus to retrieve the relative yields, in the fit to eqn (4)). From Fig. 2, the fact that within error there is reasonable agreement in the CH_2OO yields from the HCHO and the iodine atom experiments is further indication that all the sources of HCHO in each of the systems are understood and defined.

Experiments in both SO_2 and NO were performed over a range of O_2 concentrations, with measurements taken using 100% O_2 buffer gas in both cases (see Fig. 4), in order to test if O_2 has a significant effect on the CH_2OO yield. In contrast to the work of Huang *et al.*,[10] no dependence of k_{2b}/k_{2a} on $[O_2]$ was observed in any of our measurements. A fit to all our data reported here gives $k_{2b}/k_{2a} = (1.90 \pm 0.22) \times 10^{-19}$ cm^{-3}, with an intercept of (1.10 ± 0.23). Huang *et al.* noted that their observed difference in $CH_2IO_2^{\#}$ stabilisation efficiency by N_2 and O_2 was an unusual result, with N_2 and O_2 often displaying similar collisional stabilisation efficiencies. It was proposed that O_2 may not be acting as a simple collision partner to remove excess energy in $CH_2IO_2^{\#}$, but that there may be a reactive process occurring between O_2 and $CH_2IO_2^{\#}$, potentially resulting in production of HCHO, IO and O_2. However, an investigation of $CH_2I + O_2$ by Gravestock *et al.*[15] could not identify IO as a product of the reaction even when more than 10% of O_2 was present at 30 Torr total pressure, and our measurements of HCHO yields in this work are not consistent with the production of HCHO from this reaction.

At present, there does not appear to be any simple explanation as to the differences between this work and the work of Huang *et al.* in the apparent yields of CH_2OO and CH_2IO_2 from $CH_2I + O_2$ as a function of pressure. While the work of Huang *et al.* indicates a CH_2OO yield of only ~4% in air at 760 Torr, our results indicate a yield of ~18%, with potentially significant implications for the oxidation chemistry of halogen containing organic compounds and for our understanding of atmospheric chemistry in marine regions with high concentrations of species such as CH_2I_2.[26–32]

In conclusion, we have measured the yields of CH_2OO and CH_2IO_2 from the reaction of CH_2I radicals with O_2 as a function of total pressure and as a function of $[N_2]$ and $[O_2]$ using three complementary methods. Results from the three methods are similar, with no observed dependence of the CH_2OO yield on $[O_2]$. We estimate that the reaction between CH_2I and O_2 reaction has a yield of ~18% of the CH_2OO Criegee biradical at atmospheric pressure.

Acknowledgements

The authors are grateful to the National Centre for Atmospheric Science (NCAS) and the Engineering and Physical Sciences Research Council (EPSRC, grant reference EP/J010871/1) for funding.

References

1 D. Johnson and G. Marston, *Chem. Soc. Rev.*, 2008, **37**, 699–716.
2 R. Criegee and G. Wenner, *Justus Liebigs Ann. Chem.*, 1949, **564**, 9–15.
3 R. Criegee, *Angew. Chem., Int. Ed. Engl.*, 1975, **14**, 745–752.
4 C. A. Taatjes, G. Meloni, T. M. Selby, A. J. Trevitt, D. L. Osborn, C. J. Percival and D. E. Shallcross, *J. Am. Chem. Soc.*, 2008, **130**, 11883–11885.
5 O. Welz, J. D. Savee, D. L. Osborn, S. S. Vasu, C. J. Percival, D. E. Shallcross and C. A. Taatjes, *Science*, 2012, **335**, 204–207.
6 C. A. Taatjes, O. Welz, A. J. Eskola, J. D. Savee, D. L. Osborn, E. P. F. Lee, J. M. Dyke, D. W. K. Mok, D. E. Shallcross and C. J. Percival, *Phys. Chem. Chem. Phys.*, 2012, **14**, 10391–10400.
7 J. M. Beames, F. Liu, L. Lu and M. I. Lester, *J. Am. Chem. Soc.*, 2012, **134**, 20045–20048.
8 Y.-T. Su, Y.-H. Huang, H. A. Witek and Y.-P. Lee, *Science*, 2013, **340**, 174–176.
9 C. A. Taatjes, O. Welz, A. J. Eskola, J. D. Savee, A. M. Scheer, D. E. Shallcross, B. Rotavera, E. P. F. Lee, J. M. Dyke, D. K. W. Mok, D. L. Osborn and C. J. Percival, *Science*, 2013, **340**, 177–180.
10 H. Huang, A. J. Eskola and C. A. Taatjes, *J. Phys. Chem. Lett.*, 2012, **3**, 3399–3403.
11 S. Enami, T. Yamanaka, S. Hashimoto, M. Kawasaki, K. Tonokura and H. Tachikawa, *Chem. Phys. Lett.*, 2007, **445**, 152–156.
12 S. Enami, Y. Sakamoto, T. Yamanaka, S. Hashimoto, M. Kawasaki, K. Tonokura and H. Tachikawa, *Bull. Chem. Soc. Jpn.*, 2008, **81**, 1250–1257.
13 S. Enami, J. Ueda, M. Goto, Y. Nakano, S. Aloisio, S. Hashimoto and M. Kawasaki, *J. Phys. Chem. A*, 2004, **108**, 6347–6350.
14 J. Sehested, T. Ellermann and O. J. Nielsen, *Int. J. Chem. Kinet.*, 1994, **26**, 259–272.
15 T. J. Gravestock, M. A. Blitz, W. J. Bloss and D. E. Heard, *ChemPhysChem*, 2010, **11**, 3928–3941.
16 G. Hancock and V. Haverd, *Chem. Phys. Lett.*, 2003, **372**, 288–294.
17 H. M. Su, W. T. Mao and F. N. Kong, *Chem. Phys. Lett.*, 2000, **322**, 21–26.
18 U. Bley, F. Temps, H. G. Wagner and M. Wolf, *Ber. Bunsen-Ges. Phys. Chem.*, 1992, **96**, 1043–1048.
19 R. A. Alvarez and C. B. Moore, *J. Phys. Chem.*, 1994, **98**, 174–183.
20 A. J. Eskola, D. Wojcik-Pastuszka, E. Ratajczak and R. S. Timonen, *Phys. Chem. Chem. Phys.*, 2006, **8**, 1416–1424.
21 A. Masaki, S. Tsunashima and N. Washida, *J. Phys. Chem.*, 1995, **99**, 13126–13131.
22 J. C. Ianni, *Kintecus, Windows Version 2.80*, 2002, www.kintecus.com.
23 L. Vereecken, H. Harder and A. Novelli, *Phys. Chem. Chem. Phys.*, 2012, **14**, 14682–14695.

24 P. D. Lightfoot, R. A. Cox, J. N. Crowley, M. Destriau, G. D. Hayman, M. E. Jenkin, G. K. Moortgat and F. Zabel, *Atmos. Environ., Part A*, 1992, **26**, 1805–1961.

25 R. Atkinson, D. L. Baulch, R. A. Cox, J. N. Crowley, R. F. Hampson, R. G. Hynes, M. E. Jenkin, M. J. Rossi and J. Troe, *Atmos. Chem. Phys.*, 2006, **6**, 3625–4055.

26 C. M. Roehl, J. B. Burkholder, G. K. Moortgat, A. R. Ravishankara and P. J. Crutzen, *J. Geophys. Res., Atmos.*, 1997, **102**, 12819–12829.

27 L. J. Carpenter, W. T. Sturges, S. A. Penkett, P. S. Liss, B. Alicke, K. Hebestreit and U. Platt, *J. Geophys. Res., [Atmos.]*, 1999, **104**, 1679–1689.

28 L. J. Carpenter, *Chem. Rev.*, 2003, **103**, 4953–4962.

29 C. Ordonez, J. F. Lamarque, S. Tilmes, D. E. Kinnison, E. L. Atlas, D. R. Blake, G. S. Santos, G. Brasseur and A. Saiz-Lopez, *Atmos. Chem. Phys.*, 2012, **12**, 1423–1447.

30 A. Saiz-Lopez, J. M. C. Plane, A. R. Baker, L. J. Carpenter, R. von Glasow, J. C. G. Martin, G. McFiggans and R. W. Saunders, *Chem. Rev.*, 2012, **112**, 1773–1804.

31 A. Saiz-Lopez and R. von Glasow, *Chem. Soc. Rev.*, 2012, **41**, 6448–6472.

32 L. J. Carpenter, S. D. Archer and R. Beale, *Chem. Soc. Rev.*, 2012, **41**, 6473–6506.

33 T. J. Dillon, M. E. Tucceri, R. Sander and J. N. Crowley, *Phys. Chem. Chem. Phys.*, 2008, **10**, 1540–1554.